

# NLTE Model of NGC 6543's Central Star and its Relation with the Surrounding Planetary Nebula

Georgiev L. N.

*Instituto de Astronomía, Universidad Nacional Autónoma de México, CD. Universitaria, Apartado Postal 70-264, 04510 México DF, México*

georgiev@astroscu.unam.mx

and

Peimbert M.

*Instituto de Astronomía, Universidad Nacional Autónoma de México, CD. Universitaria, Apartado Postal 70-264, 04510 México DF, México*

and

Hillier D. J.

*Physics and Astronomy Department, University of Pittsburgh, 3941 O'Hara Street, Pittsburgh PA, USA*

and

Richer M. G.

*Instituto de Astronomía, Universidad Nacional Autónoma de México, CD. Universitaria, Apartado Postal 70-264, 04510 México DF, México*

Arrieta A.

*Universidad Iberoamericana, Departamento de Física y Matemáticas, Av. Prolongación Paseo de la Reforma 880, Lomas de Santa Fe, CP 01210, México, D.F., México*

and

Peimbert A.

*Instituto de Astronomía, Universidad Nacional Autónoma de México, CD. Universitaria, Apartado Postal 70-264, 04510 México DF, México*

**ABSTRACT**

We analyze the chemical composition of the central star of the planetary nebula NGC 6543 based upon a detailed NLTE model of its stellar wind. The logarithmic abundances by number are H=12.00, He=11.00, C=9.03, N=8.36, O=9.02, Si=8.19, P=5.53, S=7.57 and Fe=7.24. Compared with the solar abundances, most of the elements have solar composition with respect to hydrogen except C which is overabundant by 0.28 dex and Fe which is depleted by  $\sim 0.2$  dex. Contrary to most previous work, we find that the star is not H-poor and has a normal He composition. These abundances are compared with those found in the diffuse X-ray plasma and the nebular gas. Compared to the plasma emitting in diffuse X-rays, the stellar wind is much less depleted in iron. Since the iron depletions in the nebular gas and X-ray plasma are similar, we conclude that the plasma emitting diffuse X-rays is derived from the nebular gas rather than the stellar wind. Excellent agreement is obtained between the abundances in the stellar wind and the nebular recombination line abundances for He, C, and O relative to H. On the other hand, the derived stellar N abundance is smaller than the nebular N abundance derived from recombination lines and agrees with the abundance found from collisionally-excited lines. The mean temperature variation determined by five different methods indicates that the difference in the nebular abundances between the recombination lines and collisionally excited lines can be explained as due to the temperature variations in a chemically homogeneous medium.

*Subject headings:* stellar winds: planetary nebulae: individual(NGC 6543)

## 1. Introduction

The generally accepted scenario of planetary nebula formation is the interaction between the stellar material expelled at low velocity during the AGB phase (slow wind) and at high velocity at some later moment (fast wind; Kwok, Purton, & Fitzgerald 1978). A direct consequence of this scenario is the presence of shock fronts propagating inward into the fast wind and outward into the slow wind. The shocked gas of the fast wind should be heated to temperatures that correspond to its kinetic energy. The typical fast wind velocity is  $\sim 1000$  km/s and the mass loss rate is  $1 \times 10^{-8} M_{\odot}/\text{yr}$ , which imply temperatures  $\sim 10^7$  K. At these temperatures the gas should emit in X-rays and that emission has been detected recently (Chu et al. 2001; Guerrero et al. 2005). However, the observed temperatures of the X-ray gas are  $1 - 3 \times 10^6$  K, an order of magnitude lower than expected. Several scenarios have been proposed to explain this discrepancy (Soker & Kastner 2003), but none of them are

easily accepted as the best one.

In our previous paper (Georgiev et al. 2006), we tried to learn more of the X-ray emitting region using optical coronal lines of iron. Unfortunately, these lines were not detected, which set an upper limit to the iron composition of the X-ray emitting gas, a limit far below the solar metallicity. This result was confirmed by Kastner et al. (2006) who did not detect iron lines in their high resolution X-ray spectrum of BD+30°36939. The peculiar chemical composition of the X-ray emitting gas leads to a possible trace of its origin. If the compositions of the stellar wind, the nebula, and the X-ray emitting gas are compared, one can decide which of them are related, and that might indicate the origin of the X-ray gas and perhaps provide clues to the physical processes leading to its low temperature.

Some PNe, NGC 6543 among them, have iron abundances which are very depleted with respect to the solar value (Perinotto et al. 1999; Marcolino et al. 2007), most probably due to depletion into dust grains. The depleted iron content in both the nebular and the X-ray emitting gas points to a possible relation between them. Unfortunately, during the AGB phase of the evolution, iron atoms can capture slow neutrons (the s-processes) Busso et al. (1999). The s-processes depletes iron and one needs a good estimate of the composition of the stellar wind before arriving at any conclusion on the relation between the hot gas and its surroundings.

In this paper, we model the stellar wind of the central star of NGC 6543, one of the brightest planetary nebulae emitting X-rays, to derive its chemical composition. Section 2 presents the observed spectrum and Section 3 describes the selection of the model parameters. In Sections 4 and 5, we compare the chemical composition of the stellar wind with that of the nebular gas and the X-ray plasma, respectively. Section 6 considers the evolution of the progenitor of NGC 6543 while Section 7 presents our conclusions.

## 2. Observations

To construct a good stellar atmosphere model that includes the stellar wind, we need information from as wide a range of wavelengths as possible. We constructed the spectrum of NGC 6543’s central star from four sources, three covering the ultraviolet and one covering the optical.

First, we extracted the FUSE spectrum ( $R \sim 15000 - 20000$ ) by program Q108 (Vidal-Madjar, A) obtained on 2000 October 1 at 21h 51min. The spectrum was constructed from SiC 2A, SiC 2B, LiF 1A and LiF 1B fragments. All parts of the spectrum were shifted in wavelength and scaled to match the LiF 1B segment. The resulting spectrum was wavelength

shifted and scaled to match the overlapping part of the STIS spectrum. Second, two HST STIS spectra ( $R \sim 100000$ ) from program 9736 (P.I. R. Williams), taken on 2004 April 7, were used to cover the wavelength region from 1190 to 1500Å. Unfortunately, the third spectrum from the same program, which covers the C IV 1548/50 Å region, has a problem with the wavelength calibration and is not useful. Third, we used IUE spectrum SWP33504 ( $R \sim 10000$ ) to cover the region 1500 - 2000 Å. The two LWP high resolution spectra of NGC 6543 are too noisy and we did not use them in the diagnostic procedure. These three fractions of the spectrum were finally combined, and the resulting spectrum was used as a temperature diagnostic and for determining the reddening. After the temperature and reddening were determined, we normalized the observed spectrum to the predicted model continuum scaled to match the line free region between 1750 Å and 1900 Å.

Finally, the fourth set of spectra were in the optical and consisted of spectra obtained by us at the Observatorio Astronómico Nacional in the Sierra of San Pedro Martir (SPM) using the REOSC echelle spectrograph ( $R \sim 20000$ ). A blue spectrum was obtained on 2004 May 26. The data and their reduction are described in Georgiev et al. (2006). This spectrum was obtained to maximize S/N. All of the strong nebular lines are saturated and the spectrograph was set so that  $H_\alpha$  was outside the observed wavelength interval. Red spectra were obtained on 2004 June 6 with short exposures so that the hydrogen and oxygen lines were not saturated. The spectrum was reduced using MIDAS. After the standard CCD reductions, the spectrum was extracted only in the part of the slit covered by the star. Two additional spectra were extracted in adjoining windows. The signal from these windows was averaged, scaled, and subtracted from the stellar spectrum. As a result, most of the nebular spectrum was removed, except in the cores of the strong lines arising from both the nebula and the central star. For these stellar lines, the profiles are severely perturbed, but, keeping in mind that the stellar lines are much broader than the nebular lines, the residuals of the strong nebular lines do not affect the wings of the stellar lines, and so they may still be compared with model line profiles. This procedure worked well for the blue spectrum. The red spectrum is strongly contaminated by scattered light from  $H_\alpha$ . We corrected the spectrum for this contamination, but we expect  $H_\alpha$  to be over-corrected. Therefore, the observed intensity of  $H_\alpha$  is expected to be less than the model prediction. After the spectrum was corrected for the nebular contamination, it was normalized to the continuum by fitting polynomials to the line-free regions.

### 3. Model

The central star of NGC 6543 is known to be variable. A detailed analysis of the spectral variability was published by Prinja et al. (2007). They found that “Mostly the flux changes are at  $\sim 10$  to 20 per cent of the continuum level and occur over localized blueward velocity regions, as opposed to the flux increasing or decreasing simultaneously over the entire absorption trough.” For the rest of the spectrum the authors concluded that “Any changes in the other spectral lines are rather subtle if present at all.” Therefore, our analysis, which is based upon the overall line profile and, in most cases, on weak absorption lines, is not affected by the variability.

#### 3.1. Helium abundance

The helium content of the wind is one of the fundamental parameters which has to be determined at least roughly beforehand. The central star of NGC 6543 has been found to be “Hydrogen-poor” (Bianchi et al. 1986; de Koter et al. 1996), so we tested this assumption as the first step of our analysis. Due to the similarity of He II and H I ions, the He II lines arising from the transition  $4 - n$  with  $n$  even have wavelengths close to the wavelengths of the H I lines of the Balmer series. The lines with  $n$  odd fall between the Balmer lines and are not affected by the hydrogen component. When the wind is hydrogen-poor, the intensities of the lines with  $n$  odd and even decrease smoothly with increasing  $n$ . On the other hand, if the abundance of H I is not negligible, the intensities of the Balmer lines are higher than the He II lines with  $n$  odd (Smith 1973). From Fig. 1, it is obvious that the central star of NGC 6543 cannot be H-poor. A series of models suggest that the He/H ratio should be around solar. We adopt  $N(\text{H})/N(\text{Ne}) = 0.10$  in the following analysis.

#### 3.2. Stellar parameters

The model of a stellar wind depends upon a large number of parameters. In addition to the effective temperature and the gravity, which describe a plane parallel, static atmosphere, a wind requires parameters describing the velocity, the mass loss rate, and a parameter describing the clumpiness of the wind. The task of fitting all of the parameters is difficult. We proceeded by fixing some of the parameters while fitting the others and then iterated, changing the parameters to be fitted.

The parameters describing the star are not independent. If we describe the star as an opaque nucleus with radius  $R_*$  and temperature  $T_*$ , then its luminosity is  $L = 4\pi\sigma R_*^2 T_*^4$ . It

is known (Schmutz et al. 1989) that models with the same temperature  $T_*$ , velocity law and the same transformed radius

$$R_t = R_* \left( \frac{V_\infty/2500}{\dot{M}/10^{-8}} \right)^{\frac{2}{3}}, \quad (1)$$

have very similar emitted spectra. Substituting the radius  $R_*$ , one obtains a scaling rule for the mass loss rate if a different luminosity is necessary

$$\frac{\dot{M}_1}{\dot{M}_2} = \left( \frac{L_1}{L_2} \right)^{\frac{3}{4}}. \quad (2)$$

We describe the velocity of the wind using the standard velocity law given by

$$V(r) = V_\infty(1.0 - R/r)^\beta, \quad (3)$$

fitted to a hydrostatic atmosphere with a gravity  $\log g$ , as described in Hillier et al. (2003). The terminal velocity  $V_\infty$  was set to 1340 km/s as determined from the blue wing of the P V 1118/28 doublet. The wind of NGC 6543 is not simple. Strong lines of different ions with P Cyg profiles require different terminal velocities. Ions with higher ionization potential tend to have P Cyg lines with a more extended blue wing. In addition, Prinja et al. (2007) showed that the wind variability is present in the absorption component of P V 1118/28Å doublet but O VI 1032/38Å is more stable. The formation of the strong P Cyg lines is obviously complicated and there is no easy explanation for their behavior. We avoided this problem by excluding lines with strong P Cyg profiles from our analysis. We account for the presence of different blue wings of the P Cyg lines by increasing the error in  $V_\infty$  to 200 km/s. With the velocity law fixed, we continued with the determination of the temperature.

There are lines of several elements with two or more consecutive ionization stages which, in principle, could be used as temperature indicators. Unfortunately, it is not easy to use any of them in practice. The O IV 1339/41 Å doublet and O V 1371 Å show different terminal velocities. In addition, the O V 1371 Å line is heavily blended with iron lines and its intensity strongly depends upon the iron composition. The same is true for the N IV and N V lines. Instead of using ion ratios, we selected several temperature-sensitive features in the spectrum and searched for a temperature that reproduces most of them. These features usually depend upon the mass loss rate also, so one needs to determine the correct combination of  $T_{eff}$  and  $\dot{M}$  that reproduce the measured fluxes simultaneously. To do that, we ran a grid of models covering temperatures from 60 to 75 kK and mass loss rates from  $2.8 \times 10^{-8}$  to  $7.8 \times 10^{-8}$   $M_\odot/\text{yr}$ , setting the clumping factor to  $f = 0.1$  (see below) and the luminosity to  $L = 5200 L_\odot$  (as in previous work; de Koter et al. 1996; Georgiev et al. 2006). The temperature limits were set by the C III and P V lines. Below 60 kK the C III 1179 Å line is too strong. Above

75 kK the P V 1118/28 Å doublet is too weak. Once the grid is calculated, one can construct a surface for the value of any parameter measured in the synthetic spectra as a function of both temperature and  $\dot{M}$ . The observed value of the parameter defines an isoline on that surface. If the isolines defined by several parameters are drawn on the same coordinates  $(T_{eff}, \dot{M})$ , their crossing point defines the combination of  $T_{eff}$  and  $\dot{M}$  which reproduces all of the parameters simultaneously. In practice, the isolines do not cross in a point, but rather in a region, whose size defines the error in the parameters. We ran grids for the velocity law setting the parameter  $\beta$  equal to 1, 2 and 3. The isolines cross in a smaller region for  $\beta = 2.0$ , so we used that value in the subsequent analysis.

The left panel of Fig. 2 shows the isolines for the intensity of He II 4686Å,  $H_\beta$ , and their ratio. The right panel of the same figure shows several other diagnostics. All of the isolines cross in the vicinity of  $T = 66750 \pm 500$  K and  $\dot{M} = 3.2 \pm 0.05 \times 10^{-8} M_\odot/\text{yr}$ . We adopted these parameters for further modeling. Once the temperature and the mass loss rate are determined, the absolute flux calculated by the model can be compared with the observed UV spectrum. The difference provides an estimate of the extinction. We used the  $R$ -dependent Galactic extinction curve from Fitzpatrick (1999) for  $R = 3.1$ . The best fit of the line-free regions of the spectrum is given by  $E(B - V) = 0.025 \pm 0.005$  mag (Fig. 3) which is close enough to the value  $E(B - V) = 0.07$  mag used by Bernard-Salas et al. (2003). The error in the reddening is the formal error of the fit. The actual error is larger, due to its dependence upon the model parameters. The scaling factor between the observed UV spectrum and the calculated continuum implies a distance of  $1.81 \pm 0.05$  kpc, where the error reflects the error in the reddening. Reed et al. (1999) determined the distance to NGC 6543 of  $\sim 1.0$  kpc. To get results in agreement with this distance, we scaled down the luminosity to  $L = 1585 L_\odot$  and the mass loss rate  $\dot{M} = 1.86 \pm 0.3 \times 10^{-8} M_\odot/\text{yr}$ , according to (2), where the error also reflects the uncertainty in  $V_\infty$ . We stress that the model itself does not provide a distance due to the degeneracy between the luminosity and the mass loss rate mentioned above.

Finally, we have to address two additional parameters. First is the stellar mass. The assumed luminosity  $L = 1585 L_\odot$  and the adopted temperature implies a value of  $\log g = 5.3$  if the stellar mass is  $0.6 M_\odot$ . The mass of the star can vary by a factor of 1.3, which leads to changes in  $\log g$  of  $\pm 0.12$ . We did test runs with higher and lower gravity. There were no significant changes in the emitted spectrum, so we think that a different value of  $\log g$  (necessary for a different luminosity) would not change the conclusions made in the next section. On the other hand, the wings of the hydrogen lines are well reproduced (Fig. 5), which indicates that the adopted value of  $g$  is adequate.

Another parameter that can change the emitted spectrum is the wind clumpiness. The

winds of massive stars are clumpy, as deduced from the electron scattering wings of strong lines (Hillier 2005). The same lines in the spectrum of NGC 6543 are not strong enough to permit us to determine the clumping factor  $f$ . In general, models with the same  $\dot{M}/\sqrt{f}$  produce similar spectra. We ran test models with  $f = 0.05, 0.1, 0.5$  and  $1.0$  with corresponding changes in the mass loss rates. Only a few lines changed, between them the strong C IV 5801/12 doublet. Since we did not use these lines in the composition analysis, we set the clumping factor to  $f = 0.1$  which is similar to the value  $f = 0.08$  obtained by Prinja et al. (2007).

### 3.3. Chemical composition

Once the parameters of the star are determined, the composition of the elements is determined by comparing the predicted and observed line fluxes. As mentioned above, the strong resonance lines are poorly reproduced and are not useful for abundance determinations. The following analysis is based upon weaker lines that are formed deep in the wind and in a smaller volume. These lines are better reproduced by the model and we expect that they are less sensitive to the perturbations of the wind structure and geometry. The model reproduces most of the lines correctly, but we could not reproduce everything. Some of the observed features are missing in the model spectrum. One has to keep in mind that the model presented here includes most of the important physics and chemistry, but not all of them. Given this consideration, a comparison between observations and models with different abundances yields the errors presented in Table 2.

Oxygen is found mainly as O IV and O V. We determined its abundance using the O IV doublet at 3560/63 Å. This line is blend-free and has good S/N (Fig. 4). The line intensity is reproduced with an oxygen abundance of  $12 + \log N(\text{O})/N(\text{H}) = 9.02$  dex. As an additional criteria to check the O abundance, we used the O V 4119 Å, O V 4123 Å, and O V 5114 Å lines (Figs. 5 and 6) which were well reproduced. In addition, there are a few O V lines around 965 Å (Fig. 7) that are overestimated which points to an overabundance of O V in the model with respect to the observations. This is in agreement with the additional ionization of O V (see below) and we adopt the abundance derived from O IV lines.

In addition to the O IV and O V lines, the FUSE spectrum shows a very strong O VI 1032/38Å resonance doublet. The model with the temperature and mass loss rate adopted above underestimates these lines by an order of magnitude. One needs a temperature above 90 kK and a higher mass loss rate to reproduce this line. It is believed that the O VI 1032/38Å doublet is formed by the ionization of O V by X-ray radiation generated by internal shocks in the wind (Cassinelli et al. 1981). In support of this hypothesis, only O VI 1032/38Å is



observed and other strong O VI lines, such as the 3811/34 Å doublet, are not present in our spectra. Test models with higher a temperature, which reproduce O VI 1032/38 Å, also show an observable O VI 3811/34 Å doublet. These arguments imply an additional ionization source in the external part of the wind, which does not affect the internal, denser, part of the wind. The density in the highly-ionized part of the wind is very low meaning that only the resonance lines have enough opacity to form an observable feature, i.e., producing O VI 1032/38 Å, but not O VI 3811/34 Å. One could speculate that the additional ionization source is the diffuse X-ray plasma interior to the nebular shell. Fitting the O VI 1032/38 Å lines with shock-generated or other X-ray emission is beyond the scope of this paper. The abundance analysis based upon weak lines of low ionization stages should not be affected by the X-ray ionization and should be correct.

Carbon is represented by two ionization stages, with C IV being the dominant one. Lines of C III and C IV are observed in the FUSE, IUE, and optical regions of the spectrum. The C IV resonance doublet 1548/50 Å behaves similarly to O VI 1032/38 Å. It has a higher  $V_\infty$  and a larger observed intensity than the model predicts. We determined the carbon composition mainly from the C III 1176 Å and 977 Å lines (Figs. 9 and 7). These two lines, together with C IV 1169 Å, were used as a temperature diagnostic. Our final estimate is  $12 + \log N(\text{C})/N(\text{H}) = 9.03$  dex.

Nitrogen is mainly in the form of N V and, like O VI and C IV, it is also apparently strongly affected by the X-ray ionization. We estimate its composition using the N IV 955 Å, N IV 1718 Å, N IV 4058 Å, and N V 4944 Å lines (Figs. 7, 5, and 6, respectively). The lines are reproduced with  $12 + \log N(\text{N})/N(\text{H}) = 8.36$  dex.

The Si IV resonance doublet 1398/1402 is usually present in many objects. Due to the high temperature of the star, the lines are weak and heavily blended with Fe VI lines. Instead of using the resonance doublet, we estimated the silicon abundance using the Si IV 4089 Å and 4116 Å lines (Fig. 5). The lines are reproduced with  $12 + \log N(\text{Si})/N(\text{H}) = 8.19$  dex, a factor of five higher than the solar value. The model with this abundance reproduces several other Si IV lines as well. We have to stress that the Si IV ion is not the dominant stage of silicon at a temperature of  $\sim 70$  kK. Only 0.2% of the silicon is in Si IV. Therefore, the estimated overabundance depends strongly on the atomic data and it is highly uncertain. On the other hand, Hultzsch et al. (2007) found similar silicon overabundance in the central star of M1-37. Silicon overabundance is an unexpected result which has no explanation for the moment.

In addition to the above mentioned elements, the model contains sulfur and phosphorus. The sulfur line S V 1503 Å was fitted with  $12 + \log N(\text{S})/N(\text{H}) = 7.57$  dex. We checked that this abundance also reproduces the S VI 4162 (Fig 5) line well. The phosphorus lines P V

1118/1128 are well-fitted with an abundance of  $12 + \log N(\text{P})/N(\text{H}) = 5.53$  dex.

Finally, we analyzed the iron content. A first look at the spectrum reveals strong iron lines between 1250 Å and 1450 Å. The presence of these lines rules out a significant depletion of iron (Georgiev et al. 2006), but the precise modeling showed that these features are not very sensitive to variations in the iron abundance. A similar result was reported by Marcolino et al. (2007) for BD+30°36939. Therefore, we decided to apply the classical curve of growth method. Once we had the wind parameters and composition fixed, we ran several models with different iron abundances, starting from the solar value and finishing with 1/10 of the solar value. We selected about 10 absorption lines mainly Fe V and Fe VII (Figs. 8 and 9) that showed the strongest variation with composition. The equivalent widths of the lines both in the observed spectrum and in the models were measured using a Gaussian fit. Using the curve of growth method, we derived the Fe abundance for each line. The median value yields  $12 + \log N(\text{Fe})/N(\text{H}) = 7.24$  dex which is  $\sim 0.2$  dex lower than the solar value.

The model also includes lines of argon, neon and nickel. The abundances of these elements were set to their solar values and were not determined by line fitting.

Our elemental abundances for the central star’s wind are presented in Table 2 along with those for the Sun and the Orion nebula. Note that the Ne and Ar abundance determinations for the Orion nebula are more accurate than those for the Sun. The uncertainties in the abundances for NGC 6543, except in the case of iron, are derived from models with increased and decreased abundances. The uncertainty reflects the changes in the abundances that produce changes greater than the noise in the data. The uncertainty in the iron abundance is the standard deviation of the abundance derived for each of the lines analyzed.

Finally, we stress that our model of the central star’s wind is undoubtedly only one of several possible solutions. Several combinations of parameters produce similar spectra and therefore increases the uncertainty in the stellar parameters, which is reflected by the errors in the derived abundances. In addition, the observed spectrum shows features that are not present in our model. Nonetheless, the precision of the chemical composition presented here is sufficiently robust for the purposes of this paper. A more refined model, dealing with the formation of O VI lines, the identification of the observed features and the difference in the wind velocity shown by different resonance lines will be treated in a forthcoming paper. A final conclusion on the evolutionary status of the object and the interrelation between its components (star, nebula, X-ray emitting gas) require a self consistent model including the central star and the nebula (Morisset & Georgiev, in preparation).

#### 4. Relationship between the stellar and nebular abundances

In most planetary nebulae, the abundances for heavy elements derived from recombination and collisionally-excited lines do not agree. Explanations for this result depend fundamentally upon large temperature variations that cannot be explained by simple photoionization models (e.g., Liu 2006; Peimbert & Peimbert 2006, and references therein). The temperature variations explain the large differences between the chemical abundances derived from recombination lines and those derived from collisionally excited lines when a constant temperature is used. The difference between both types of abundances is called the abundance discrepancy factor,  $ADF$ . There are two different ideas to explain the  $ADF$ 's: (a) the presence of temperature variations in a chemically inhomogeneous medium (e. g. Torres-Peimbert et al. 1990; Liu 2006, and references therein), and (b) the presence of temperature variations due to other causes in a chemically homogeneous medium (e. g. Peimbert & Peimbert 2006, and references therein).

According to the two-abundance nebular model by Liu and collaborators, PNe present two components: (a) a low density component that has most of the mass and is relatively hot, emits practically all the intensity of the H lines and of the forbidden lines in the visual and the UV, as well as part of the intensity of the He I lines, and (b) a high density component that has only a small fraction of the total mass, is relatively cool, H-poor, rich in heavy elements, emits part of the He I and all of the recombination lines of the heavy elements, but emits practically no H nor any collisionally-excited lines from heavy elements. Chemically inhomogeneous nebulae can be produced by H-poor stars that eject H-poor material into H-rich nebulae. That is the case in A30 and A78 (Jacoby 1979; Hazard et al. 1980; Jacoby & Ford 1983; Manchado et al. 1988; Wesson et al. 2003). This type of situation might occur in those cases where the central star has an H-poor atmosphere. According to Górny & Tylenda (2000) about 10% of the central stars of PNe are H-poor. Studies based upon the Sloan project find similar results: based upon 2065 DA and DB white dwarfs, Kleinman et al. (2004) find that 1888 are non magnetic DAs and 177 are non magnetic DBs. Therefore, we conclude that about 10% of Galactic PNe have a H-poor central star, and might show He, C, and O rich inclusions in their expanding shells. We consider it unlikely that PNe with H-rich central stars would contain significant amounts of H-poor material in their associated nebulae.

##### 4.1. Nebular collisional and recombination abundances

In Table 3, we present abundances derived from collisionally-excited lines from different studies. In the last column, we present our adopted values based upon the values presented

in the previous columns. For  $O^{++}$ , the value taken from Wesson & Liu (2004) is based only upon their [O III]  $\lambda 4959$  determination, since the  $\lambda\lambda$  52 and 88  $\mu\text{m}$  lines have a different dependence upon the temperature than the [O III]  $\lambda\lambda 4959$  and 5007 lines. Also, the presence of density variations affects the O abundance determination based on the  $\lambda\lambda$  52 and 88  $\mu\text{m}$  lines.

In Table 4, we present abundances derived from recombination lines from different studies. In the last column we present our adopted values. The  $N(\text{He})/N(\text{H})$  ratio was derived by us from helium recombination lines and using more recent atomic data than those used in other studies. The detailed abundance determination is based upon maximum likelihood method, MLM, and is discussed in section 4.2. For C, the adopted value is just the average of the three determinations. For  $O^{++}$ , the adopted abundance value is based upon the determination of Wesson & Liu (2004), but with two modifications: (a) we weighted the contribution of each multiplet according to its effective recombination coefficient, and (b) we eliminated multiplet V12 that might be contaminated by other emission lines. Our determination yields  $N(O^{++})/N(H^+) = 1.42 \times 10^{-3}$ . Note that V1, the brightest multiplet, yields  $1.18 \times 10^{-3}$  for this ratio. Adopting an ionization correction factor of 1.09 derived from the [O II]  $\lambda\lambda$  3726,3729 lines and the  $N(O^{++})/N(H^+)$  recombination ratio, we obtain an oxygen abundance  $12 + \log N(\text{O})/N(\text{H}) = 9.19$  dex. At first sight the Ne/H ratio derived from recombination lines seems to be high (see Table 4), but the values for  $\log \text{Ne}/\text{O}$  values for the CELs and RLs amount to -0.52 and -0.54 dex, respectively, in good agreement with the values derived for a large number of PNe by Torres-Peimbert & Peimbert (1977) and Kingsburgh & Barlow (1994), who find an average  $\log \text{Ne}/\text{O}$  ratio of -0.59 dex.

#### 4.2. $t^2$ value determinations

In Table 5, we present various temperature determinations for NGC 6543.  $T(\text{Bac})$  is the temperature determined from the intensity ratio of the Balmer continuum to a Balmer line.  $T(\text{He II})$  is the temperature derived from the He I recombination lines (see next subsection).  $T[\text{O III}]$  and  $T[\text{O II}]$  are the temperatures derived from the ratio of the auroral and nebular line intensities for the corresponding ions.  $T([\text{O III}],[\text{O II}])$  is the representative temperature for the forbidden lines, where we are assuming that 92% of the emission originates in the  $O^{++}$  zone and 8% in the  $O^+$  zone. The differences among the various temperatures imply the presence of temperature variations within the observed volume. Also, the differences between the collisional and recombination abundances, the  $ADF$  values, for C, N, O, and Ne also imply the presence of temperature variations.

To reconcile the differences among the various temperatures and between the collisional

and recombination abundances it is possible to characterize the temperature structure by an average temperature,  $T_0$  and a mean square temperature variation,  $t^2$ . These quantities are given by

$$T_0(N_e, N_i) = \frac{\int T_e(r) N_e(r) N_i(r) dV}{\int N_e(r) N_i(r) dV} \quad (4)$$

and

$$t^2 = \frac{\int (T_e - T_0)^2 N_e N_i dV}{T_0^2 \int N_e N_i dV} \quad (5)$$

where  $N_e$  and  $N_i$  are the electron and the ion densities, respectively, of the observed emission line and  $V$  is the observed volume (Peimbert 1967).

Under the assumption of chemical homogeneity to derive a  $t^2$  value, we need two independent temperature determinations, and the temperature dependence of the line or continuum intensities used to derive the temperature. It is also possible to derive a  $t^2$  value for a particular ion by reconciling the abundances derived for this ion derived from the intensities of collisional and recombination lines (Peimbert et al. 2004, and references therein). The result is correct even in the presence of chemical inhomogeneities.

In Table 6, we present five independent  $t^2$  determinations. The first two were obtained from the comparison of two temperatures representative of the whole observed volume, and the other three were derived under the assumption that the collisional and the recombination abundances had to be the same. The temperature dependencies of the recombination lines of  $C^{++}$ ,  $O^{++}$ , and  $Ne^{++}$ , needed to determine the  $t^2$  values were obtained from Davey et al. (2000), Storey (1994), and Kisielius et al. (1998), respectively.

### 4.3. Physical conditions derived from the helium recombination lines

To obtain  $N(He^+)/N(H^+)$  values, we need a set of effective recombination coefficients for the helium and hydrogen lines, an estimate of the optical depth effects for the He I lines, and the contribution to the He I line intensities due to collisional excitation. We used the hydrogen recombination coefficients from Storey & Hummer (1995), the helium recombination coefficients from Porter et al. (2005), with the interpolation formulae provided by Porter et al. (2007), and the collisional contribution to the He I lines by Sawey & Berrington (1993) and Kingdon & Ferland (1995). The optical depth effects in the triplet lines were estimated from the computations by Benjamin et al. (2002).

To derive the physical conditions associated with the helium ionized region, we have used a maximum likelihood method, MLM (Peimbert et al. 2000, 2002). To determine,  $N_e(He\ II)$ ,  $T_e(He\ II)$ ,  $N(He^+)/N(H^+)$ , and the optical depth in the He I 3889 Å line, ( $\tau_{3889}$ ),

self-consistently, we used as inputs a characteristic density from the forbidden line ratios of  $N_e = 4000 \pm 2000 \text{ cm}^{-3}$  and 13  $I(\text{He I})/I(\text{H I})$  line ratios observed by Wesson & Liu (2004, the 13 He I lines are  $\lambda\lambda$  3820, 3889, 3965, 4026, 4387, 4438, 4471, 4713, 4922, 5876, 6678, 7065, and 7281). Each of the 14 observational constraints depends upon  $T_e(\text{He II})$ ,  $N_e(\text{He II})$ ,  $N(\text{He}^+)/N(\text{H}^+)$ , and  $\tau_{3889}$ , each dependence being unique. Therefore, we have a system of 14 equations and 4 unknowns. We obtain the best value for the 4 unknowns and  $t^2$  by minimizing  $\chi^2$ . In this way, we obtained that  $t^2 = 0.035 \pm 0.014$ ,  $T_e(\text{He II}) = 6674 \pm 559 \text{ K}$ ,  $N_e(\text{He II}) = 3383 \pm 2100 \text{ cm}^{-3}$ ,  $\tau_{3889} = 9.4 \pm 0.9$ , and  $N(\text{He}^+)/N(\text{H}^+) = 0.1130 \pm 0.0023$ .

#### 4.4. Comparison of stellar and nebular abundances

In Table 7, we present the stellar abundances for NGC 6543 based upon the non-LTE model and compare them with the nebular abundances derived from recombination lines (RL) and collisionally excited lines (CEL). The agreement between the nebular recombination line abundances and the stellar abundances for He, C, and O is excellent, which indicates that the central star is not ejecting H-poor material into the nebula, material that is needed to support the two-abundances nebular model. From the five independent  $t^2$  values, we conclude that the temperature structure for H, He, C, O, and Ne is similar and therefore that the proper heavy element abundances to compare with those of H and He are those derived from recombination lines. This conclusion is reasonable because the temperature dependence of the recombination lines of the five elements is weak and similar. Consequently, the presence of temperature variations does not affect the derived abundances. The opposite is the case when comparing collisionally excited lines with recombination lines because their temperature dependence is very different (e. g. Peimbert 1967). In other words, the *ADF's* in NGC 6543 are solely due to temperature variations in a medium where H, He, C, O, and Ne are homogeneously distributed. Our results are in disagreement with the conclusions of Wesson & Liu (2004) who propose that this object contains high-density, H-poor inclusions that are rich in helium and heavy elements.

### 5. Comparison of the abundances in the stellar wind and the X-ray plasma

Iron depletion in a hydrogen-rich CSPN is an unexpected result. It is generally believed that H-poor star are also iron-poor, but that H-rich stars have normal iron content (Miksa et al. 2002; Herald & Bianchi 2004a,b,c; Stasinska et al. 2004). As Figs. 8 and 9 show, some of the iron lines are well-reproduced, and the equivalent width of others is over-estimated. As a result, it seems clear that we may reject a solar iron composition for the

stellar wind of the central star in NGC 6543. Nonetheless, the depletion of iron is moderate.

In our previous paper (Georgiev et al. 2006), we showed that the X-ray-emitting plasma in NGC 6543 is heavily depleted in iron. This chemical peculiarity allows one to determine the origin of this plasma by comparison with the iron abundances in the stellar wind and the nebular gas. In other words, are the X-rays emitted by the shocked stellar wind, whose temperature is reduced by some mechanism (for proposed scenarios, see Soker & Kastner 2003), or are the X-rays emitted by heated nebular gas? We find that the wind from the central star is depleted in iron, but by a factor of only 1.6 with respect to the solar iron abundance. The depletion needed to explain the missing [Fe XIV] 5303 Å line in the X-ray plasma is at least a factor of 10. As a result, the X-ray emitting gas cannot be related to the stellar wind. On the other hand, the nebular gas is iron-depleted. The iron abundance in the nebular gas is estimated to be depleted by a factor of 11 compared to the solar abundance (Perinotto et al. 1999). Therefore, the hot gas appears to be of nebular origin.

At least for NGC 6543, therefore, one can interpret the formation of the hot, X-ray-emitting plasma as the result of heating nebular material. One possible mechanism to accomplish this is thermal conduction, as suggested by Soker (1994) and Zhekov & Perinotto (1996, 1998). This mechanism also explains the low temperature of the X-ray emitting gas. In this case, the observed temperature is not directly related to the deposition of the mechanical energy by the wind, but rather to the efficiency of thermal conduction. The cold nebular gas is heated by thermal conduction to the observed temperature of the hot plasma and so emits in diffuse X-rays.

The same scenario can be extended to at least one other object with diffuse X-ray emission. Marcolino et al. (2007) showed that the central star of BD+30°3639 has an iron abundance that is only moderately depleted. They concluded that the iron forest in the UV is reproduced with an iron content equal to 1/4 of the solar value, but they cannot rule out the solar composition either. Previously, we have found the X-ray-emitting plasma to be depleted in iron by a factor of 8 (Georgiev et al. 2006). This result again implies that the hot gas arises from nebular material rather than from the stellar wind.

## 6. The evolution of the progenitor of NGC 6543

In addition to the iron abundance in the stellar wind, we derive the abundances of CNO and some other elements that constrain the evolution of the star before it became a planetary nebula. The most important abundance anomaly is the carbon abundance. Compared to the solar composition, carbon is enriched significantly, while oxygen and nitrogen are almost

normal. In addition, iron is depleted. These abundances imply that the progenitor star had a mass below  $4.0 M_{\odot}$ , but higher than  $1.8 M_{\odot}$ . The upper limit follows from the normal nitrogen composition. Stars with masses above  $4.0 M_{\odot}$  experience hot bottom burning and show large nitrogen and helium enhancements (Herwig 2005). On the other hand, carbon is overabundant, which requires a carbon-rich intershell, formed only in stars with masses above  $1.8 M_{\odot}$ . The depletion of iron points to the presence of effective s-processes. We cannot observe any of the elements heavier than iron and cannot determine their abundances, but the iron depletion is an indirect indicator of these processes.

## 7. Conclusions

We have obtained a detailed atmospheric NLTE model of the central star of NGC 6543 that includes a stellar wind and that matches a large number of the observed emission and absorption lines. The main physical parameters of the model are:  $T_{eff} = 66750$  K,  $R_{star} = 1.97 \times 10^{10}$  cm,  $L = 1585 L_{\odot}$ ,  $\log g = 5.3$  cm s $^{-2}$ ,  $\dot{M} = 1.86 \times 10^{-8} M_{\odot}/\text{yr}$  (adopting a clumping factor  $f = 0.1$ ), and  $V_{\infty} = 1340$  km/sec. For this model we assumed a distance of 1 kpc. Changes in the distance and the mass of the central star affect the value of  $\log g$  but do not appreciably modify the spectrum or the chemical abundances that we derive. The chemical composition of the stellar wind is presented in Table 2. The He/H ratio has been reliably determined and implies that the central star is not He-rich, contrary to the results obtained by most other authors.

The chemical composition of the stellar wind may be compared with the compositions of other components in the planetary nebula system. In particular, the iron abundance in the stellar wind is much higher than that found for the nebular gas or the hot plasma that emits in X-rays. Therefore, it would appear that the plasma emitting diffuse X-rays in NGC 6543 must arise from heated nebular material. The same conclusion is reached regarding the X-ray-emitting plasma in BD+30°3639.

We have also derived the chemical composition of the nebula surrounding the star based upon recombination lines (RL) and collisionally excited lines (CEL). The abundances of C, O, and Ne relative to hydrogen derived from recombination lines are from 0.4 to 0.5 dex higher than the abundances derived from collisionally excited lines. The difference has been called the *ADF*. From five different methods involving emission lines of H, He, C, O, and Ne, we have found a mean square temperature variation  $t^2 = 0.028 \pm 0.005$ . Supposing spatial temperature variations of this amplitude in a chemically homogeneous nebula, it is possible to reconcile the CEL and RL abundances. In this situation, we find excellent agreement between the stellar and the nebular RL abundances for He/H, C/H, and O/H. On the other



hand, the stellar N/H value is about 0.4 dex smaller than the nebular RL abundance and agrees with the nebular CEL abundance.

This is the first paper where we make a detailed comparison between the chemical composition of the central star and of the surrounding nebula of a planetary nebula. We consider it imperative to compare the chemical composition of the central stars of planetary nebulae with those of their surrounding nebulae to advance the study of the evolution of intermediate mass stars. This comparison is also paramount to test different hypotheses regarding the origin of a variety of observed properties, among them the large temperature variations present in many planetary nebulae and the origin of the X-ray emission.

It is a pleasure to acknowledge Svetozar Zhekov for useful discussions. This work was partly supported by the CONACyT grants 60967, 46904 and 42809 and UNAM DGAPA grants IN115807, IN108406, and IN108506.

Facilities: FUSE, HST(STIS), IUE. SPM

## REFERENCES

- Asplund, M., Grevesse, N., & Sauval, A. J. 2005, *Cosmic Abundances as Records of Stellar Evolution and Nucleosynthesis*, 336, 25
- Benjamin, R. A., Skillman, E. D., & Smits, D. P. 2002, *ApJ*, 569, 288
- Bernard-Salas, J., Pottasch, S. R., Wesselius, P. R., & Feibelman, W. A. 2003, *A&A*, 406, 165
- Bianchi, L., Cerrato, S., & Grewing, M. 1986, *A&A*, 169, 227
- Busso, M., Gallino, R., & Wasserburg, G. J. 1999, *ARA&A*, 37, 239
- Cassinelli, J. P., Waldron, W. L., Sanders, W. T., Harnden, F. R., Jr., Rosner, R., & Vaiana, G. S. 1981, *ApJ*, 250, 677
- Castor, J. I., Lutz, J. H., & Seaton, M. J. 1981, *MNRAS*, 194, 547
- Chu, Y.-H., Guerrero, M. A., Gruendl, R. A., Williams, R. M., & Kaler, J. B. 2001, *ApJ*, 553, L69
- Davey, A. R., Storey, P. J., & Kisielius, R. 2000, *A&AS*, 142, 85

- Esteban, C., Peimbert, M., García-Rojas, J., Ruiz, M. T., Peimbert, A., & Rodríguez, M. 2004, *MNRAS*, 355, 229
- Fitzpatrick, E. L. 1999, *PASP*, 111, 63
- Georgiev, L. N., Richer, M. G., Arrieta, A., & Zhekov, S. A. 2006, *ApJ*, 639, 185
- Georgiev, L. N., Hillier, D. J., Richer, M. G., & Arrieta, A. 2006, *Planetary Nebulae in our Galaxy and Beyond*, 234, 401
- Górny, S. K., & Tylenda, R. 2000, *A&A*, 362, 1008
- Guerrero, M. A., Chu, Y.-H., & Gruendl, R. A. 2005, *Planetary Nebulae as Astronomical Tools*, 804, 157
- Hazard, C., Terlevich, R., Ferland, G., Morton, D. C., & Sargent, W. L. W. 1980, *Nature*, 285, 463
- Herald, J. E., & Bianchi, L. 2004a, *ApJ*, 609, 378
- Herald, J. E., & Bianchi, L. 2004b, *ApJ*, 611, 294
- Herald, J. E., & Bianchi, L. 2004c, *PASP*, 116, 391
- Herwig, F. 2005, *ARA&A*, 43, 435
- Hillier, D. J., Lanz, T., Heap, S. R., Hubeny, I., Smith, L. J., Evans, C. J., Lennon, D. J., & Bouret, J. C. 2003, *ApJ*, 588, 1039
- Hillier, D. J. 2005, *The Fate of the Most Massive Stars*, 332, 215
- Hultsch, P. J. N., Puls, J., Méndez, R. H., Pauldrach, A. W. A., Kudritzki, R.-P., Hoffmann, T. L., & McCarthy, J. K. 2007, *A&A*, 467, 1253
- Jacoby, G. H. 1979, *PASP*, 91, 754
- Jacoby, G. H., & Ford, H. C. 1983, *ApJ*, 266, 298
- Kastner, J. H., Sam Yu, Y., Houck, J., Behar, E., Nordon, R., & Soker, N. 2006, *Planetary Nebulae in our Galaxy and Beyond*, 234, 169
- de Koter, A., Hubeny, I., Heap, S. R., & Lanz, T. 1996, *Hydrogen Deficient Stars*, 96, 141
- Kingdon, J., & Ferland, G. J. 1995, *ApJ*, 442, 714

- Kingsburgh, R. L., & Barlow, M. J. 1994, MNRAS, 271, 257
- Kingsburgh, R. L., Lopez, J. A., & Peimbert, M. 1996, Cosmic Abundances, 99, 350
- Kleinman, S. J., et al. 2004, ApJ, 607, 426
- Kisielius, R., Storey, P. J., Davey, A. R., & Neale, L. T. 1998, A&AS, 133, 257
- Kwok, S., Purton, C. R., & Fitzgerald, P. M. 1978, ApJ, 219, L125
- Liu, X.-W. 2006, Planetary Nebulae in our Galaxy and Beyond, 234, 219
- Manchado, A., Mampaso, A., & Pottasch, S. R. 1988, A&A, 191, 128
- Marcolino, W. L. F., Hillier, D. J., de Araujo, F. X., & Pereira, C. B. 2007, ApJ, 654, 1068
- Miksa, S., Deetjen, J. L., Dreizler, S., Kruk, J. W., Rauch, T., & Werner, K. 2002, A&A, 389, 95
- Peimbert, A., Peimbert, M., & Luridiana, V. 2002, ApJ, 565, 668
- Peimbert, M. 1967, ApJ, 150, 825
- Peimbert, M., Torres-Peimbert, S., & Luridiana, V. 1995, Revista Mexicana de Astronomia y Astrofisica, 31, 131
- Peimbert, M., Peimbert, A., & Ruiz, M. T. 2000, ApJ, 541, 688
- Peimbert, M., Peimbert, A., Ruiz, M. T., & Esteban, C. 2004, ApJS, 150, 431
- Peimbert, M., & Peimbert, A. 2006, Planetary Nebulae in our Galaxy and Beyond, 234, 227
- Perinotto, M., Cerruti-Sola, M., & Lamers, H. J. G. L. M. 1989, ApJ, 337, 382
- Perinotto, M., Bencini, C. G., Pasquali, A., Manchado, A., Rodriguez Espinosa, J. M., & Stanga, R. 1999, A&A, 347, 967
- Porter, R. L., Bauman, R. P., Ferland, G. J., & MacAdam, K. B. 2005, ApJ, 622, L73
- Porter, R. L., Ferland, G. J., & MacAdam, K. B. 2007, ApJ, 657, 327
- Prinja, R. K., Hodges, S. E., Massa, D. L., Fullerton, A. W., & Burnley, A. W. 2007, MNRAS, 882
- Reed, D. S., Balick, B., Hajian, A. R., Klayton, T. L., Giovanardi, S., Casertano, S., Panagia, N., & Terzian, Y. 1999, AJ, 118, 2430

- Rola, C., & Stasinska, G. 1994, *A&A*, 282, 199
- Sawey, P. M. J., & Berrington, K. A. 1993, *Atomic Data and Nuclear Data Tables*, 55, 81
- Schmutz, W., Hamann, W.-R., & Wessolowski, U. 1989, *A&A*, 210, 236
- Smith, L. F. 1973, *Wolf-Rayet and High-Temperature Stars*, 49, 15
- Soker, N. 1994, *AJ*, 107, 276
- Soker, N., & Kastner, J. H. 2003, *ApJ*, 583, 368
- Stasińska, G., Grafener, G., Pea, M., Hamann, W.-R., Koesterke, L., & Szczerba, R. 2004, *A&A*, 413, 329
- Storey, P. J. 1994, *A&A*, 282, 999
- Storey, P. J., & Hummer, D. G. 1995, *MNRAS*, 272, 41
- Torres-Peimbert, S. & Peimbert, M., 1977, *Revista Mexicana de Astronomia y Astrofisica*, 2, 181
- Torres-Peimbert, S., Peimbert, M., & Pena, M. 1990, *A&A*, 233, 540
- Wesson, R., Liu, X.-W., & Barlow, M. J. 2003, *MNRAS*, 340, 253
- Wesson, R., & Liu, X.-W. 2004, *MNRAS*, 351, 1026
- Zhang, Y., Liu, X.-W., Wesson, R., Storey, P. J., Liu, Y., & Danziger, I. J. 2004, *MNRAS*, 351, 935
- Zhang, Y., Liu, X.-W., Liu, Y., & Rubin, R. H. 2005, *MNRAS*, 358, 457
- Zhekov, S. A., & Perinotto, M. 1996, *A&A*, 309, 648
- Zhekov, S. A., & Perinotto, M. 1998, *A&A*, 334, 239

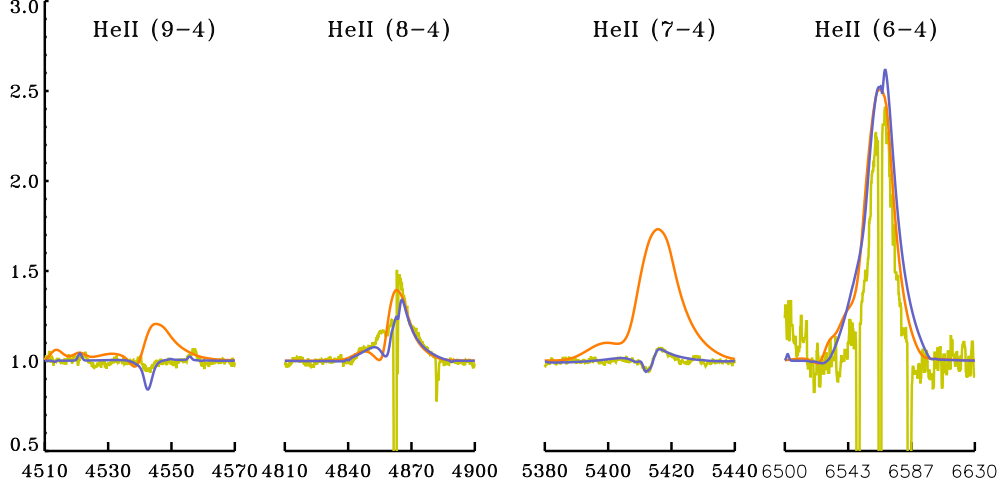


Fig. 1.— H I and He II lines from transition  $n - 4$ . The orange line represents the model with no hydrogen. The blue line represents the model with  $\text{He}/\text{H} = 0.10$ . The observations are represented with the green line. Clearly, the H-poor model overestimates the intensities of the lines with  $n$  odd.

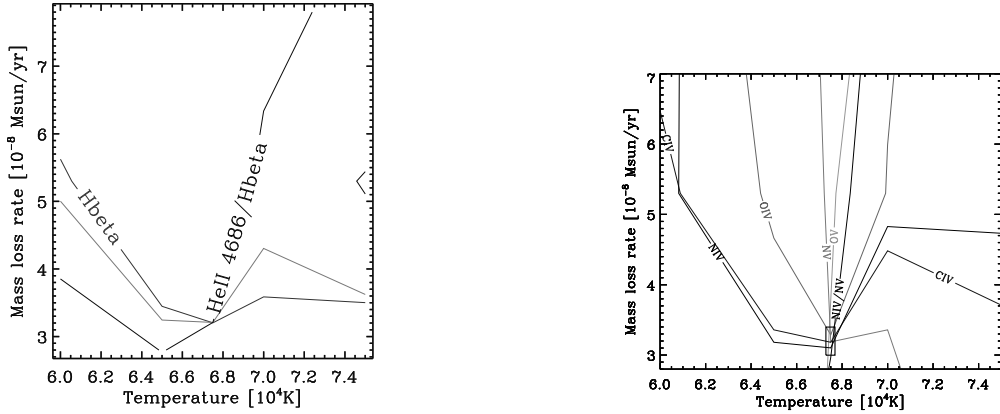


Fig. 2.— Contour lines of the equivalent width of the lines from several ions plotted on a grid of 15 models (see text). Left panel:  $\text{H}\beta$ , He II 4686 and  $\text{I}(\text{H}\beta)/\text{I}(\text{He II 4686})$  (dotted line). Right panel: C IV 5802, O IV 3563, O V 4930, N IV 955 and N V 4944 lines.

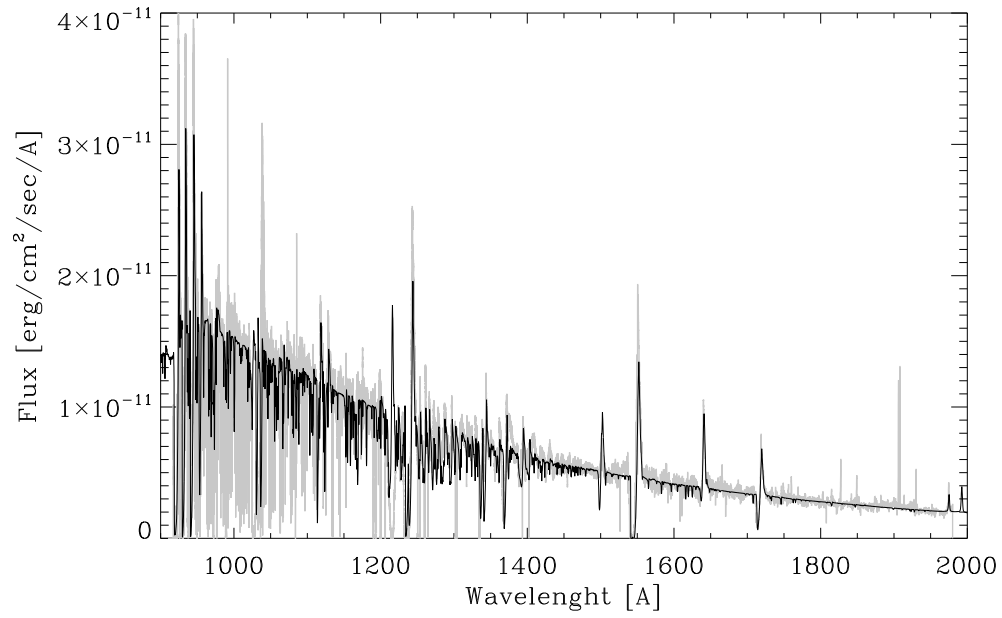


Fig. 3.— Comparison of the observed absolute UV flux (gray) with that predicted by the model (black), adopting a reddening of  $E(B - V) = 0.025$  mag and a distance of 1 kpc

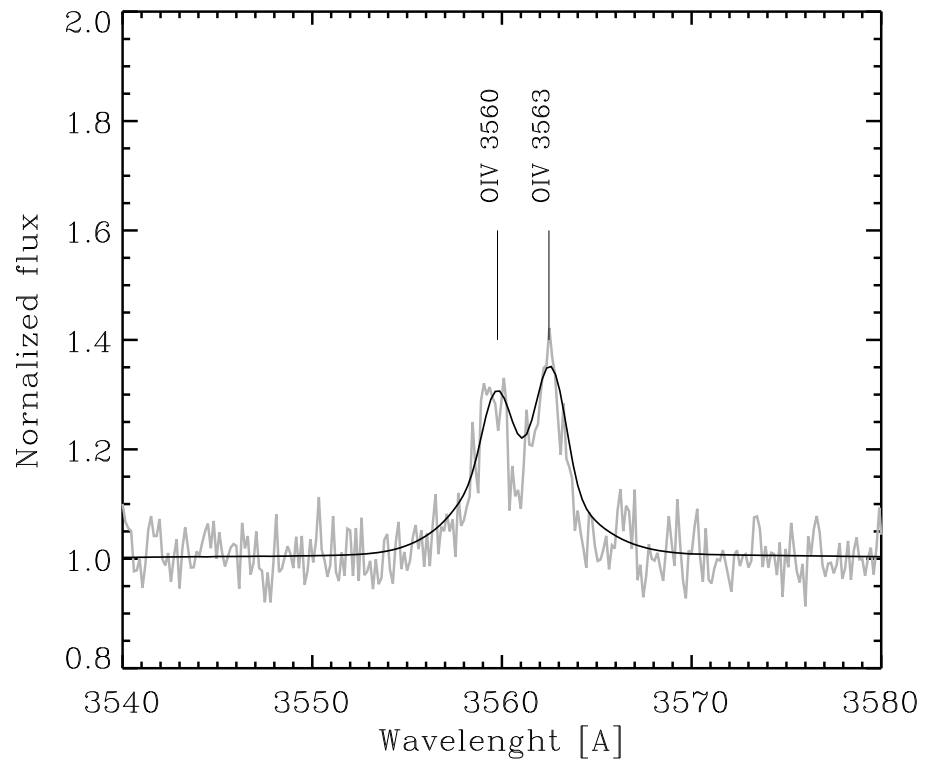


Fig. 4.— The fit to the O IV 3560/63 Å doublet.

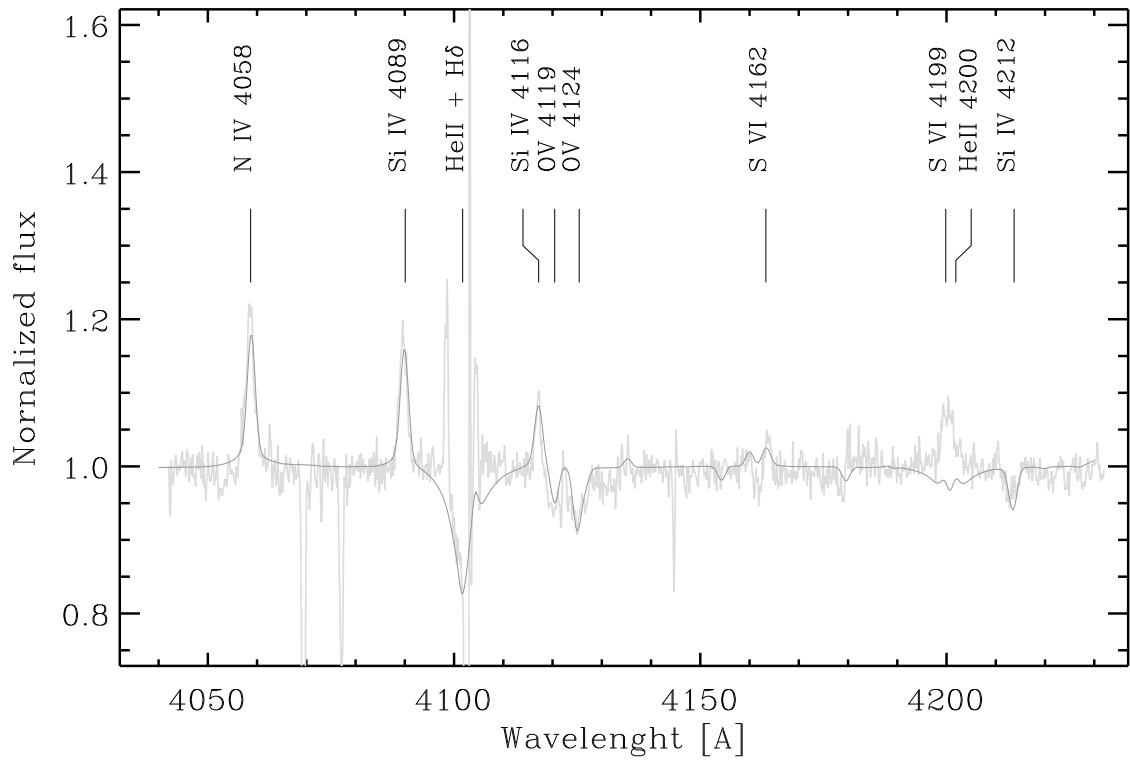


Fig. 5.— Comparison of the observed spectrum and the model. The Si IV lines are reproduced with an enhanced silicon abundance.



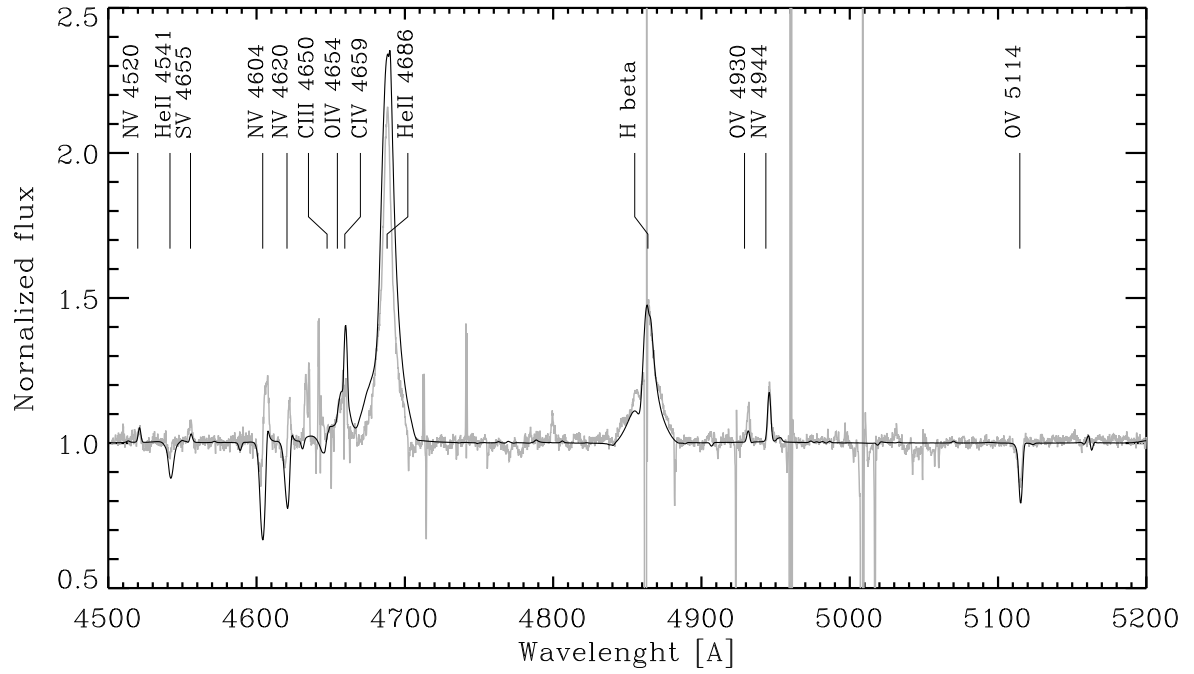


Fig. 6.— Comparison of the observed spectrum and the model. Most of the lines are well reproduced, except N V 4604/20, though note that N V 4944 is reproduced.

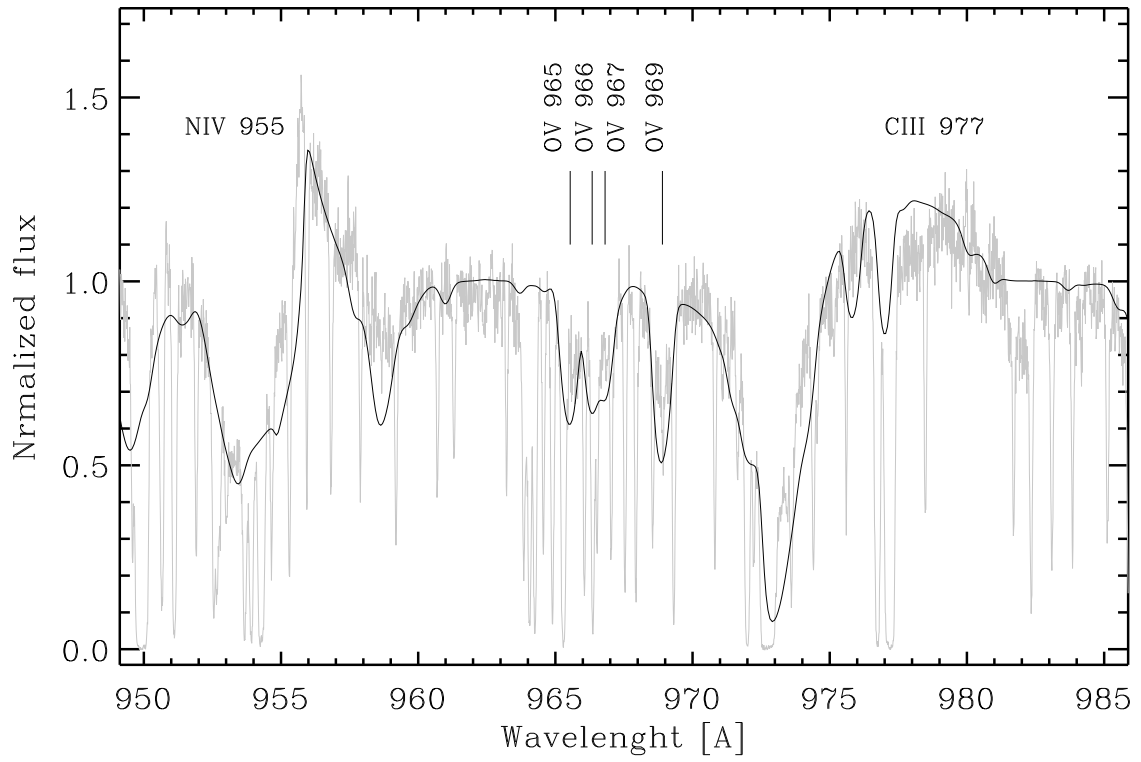


Fig. 7.— Comparison of the observed spectrum and the model in the FUV.

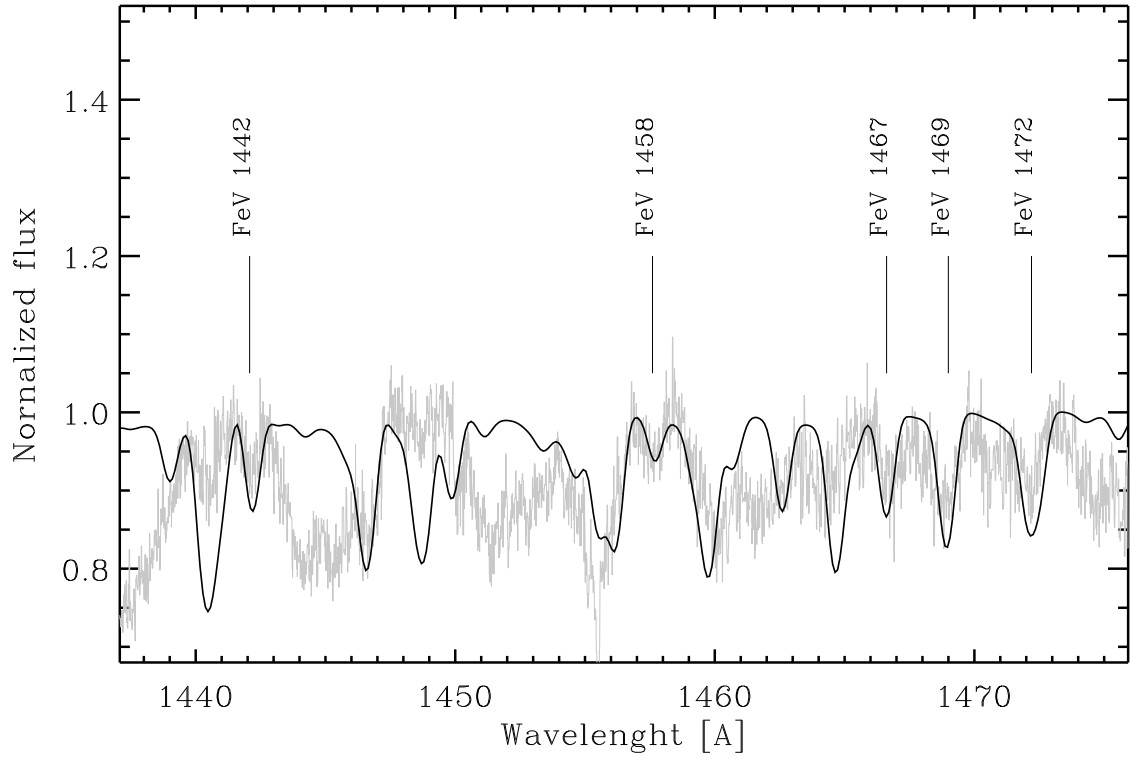


Fig. 8.— Lines used for measuring the iron composition. The Fe V lines are marked.

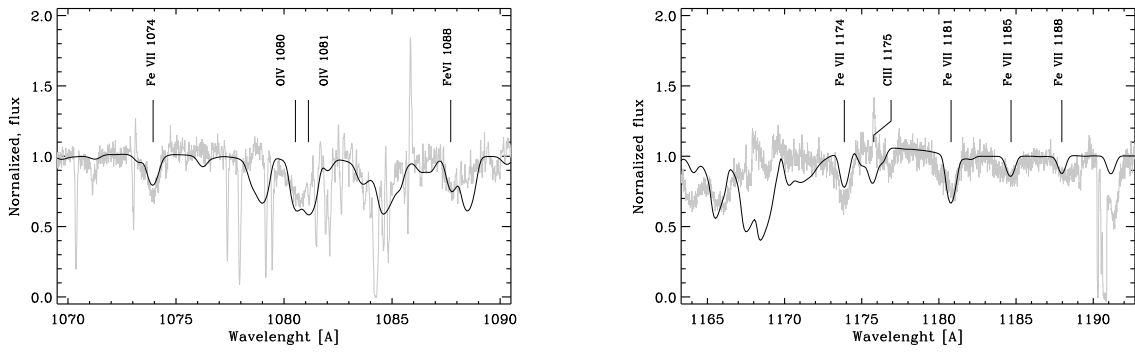


Fig. 9.— Lines used for measuring the iron composition. A variety of lines are marked.

Table 1. Comparison of the stellar parameters obtained by different authors

Reference	$V_{\infty}[km/s]$	$\beta$	$T_{eff}[K]$	$L/L_{\odot}$	Distance, [pc]	$\dot{M}[M_{\odot}/yr]$
Castor et al. (1981)	2150	1.0	43000	2000	1170	$9 \times 10^{-8}$
Bianchi et al (1986)	1900	2.0	80000	15100	1390	$32 \times 10^{-8}$
Perinotto et al. (1989)	1900	1.5	60000	5600	1440	$4 \times 10^{-8}$
de Koter et al. (1996)	1600	1.5	48000	5200	-	$16 \times 10^{-8}$
this work	1340	2.0	66750	1585	1000	$1.86 \times 10^{-8}$

Table 2. Derived stellar abundances

Element	X/H	12+ Log $N(X)/N(H)$	Sun <sup>a</sup>	[X/O] <sup>b</sup>	Orion Nebula <sup>c</sup>
He	0.1	11.00±0.04	10.93±0.01	...	10.988±0.003
C	1.060E-03	9.03±0.10	8.39±0.05	+0.28±0.1	8.52±0.02
N	2.292E-04	8.36±0.10	7.78±0.06	+0.22±0.1	7.73±0.09
O	1.055E-03	9.02±0.04	8.66±0.05	0.00	8.73±0.03
Si	1.553E-04	8.19±0.20	7.51±0.04	+0.32±0.2	...
Ne	...	...	7.84±0.04	...	8.05±0.07
P	3.390E-07	5.53±0.10	5.36±0.04	-0.19±0.1	...
S	3.693E-05	7.57±0.10	7.14±0.05	0.07±0.1	7.22±0.04
Ar	...	...	6.18±0.08	...	6.62±0.04
Fe	1.750E-05	7.24±0.10	7.45±0.05	-0.57±0.1	...

<sup>a</sup>Asplund et al. (2005).

<sup>b</sup>[X/O] = log(X/O)-log(X/O)<sub>⊙</sub>

<sup>c</sup>Esteban et al. (2004).

Table 3. Nebular collisional abundances <sup>a</sup>

Element	(1)	(2)	(3)	(4)	(5)
C	8.50	8.40	...	8.30	8.40 ± 0.10
N	8.50	8.36	...	...	8.79 ± 0.06
Ne	8.27	8.28	8.20	...	8.25 ± 0.06
S	7.09	7.11	7.05	...	7.08 ± 0.06
Ar	6.53	6.62	...	...	6.57 ± 0.06
Cl	5.40	...	...	...	5.40 ± 0.10

<sup>a</sup>In units of 12+ Log  $N(X)/N(H)$ . 1 Zhang et al. (2004); 2 Bernard-Salas et al. (2003); 3 Kingsburgh et al. (1996); 4 Rola & Stasinska (1994) and Peimbert et al. (1995); 5 adopted values.

Table 4. Nebular recombination abundances <sup>a</sup>

Element	(1)	(2)	(3)	(4)	(5)	(6)
He	11.07	11.07	11.09	...	11.05	11.05 ± 0.01
C	8.90	...	8.92	8.87	...	8.90 ± 0.10
N	8.83	...	...	...	...	8.83 ± 0.20
O	9.30	...	9.40	...	9.19	9.19 ± 0.12
Ne	8.67	...	...	...	...	8.67 ± 0.10

<sup>a</sup>In units of  $12 + \log N(X)/N(H)$ . 1 Wesson & Liu (2004); 2 Bernard-Salas et al. (2003); 3 Kingsburgh et al. (1996); 4 Rola & Stasinska (1994) and Peimbert et al. (1995); 5 this paper; 6 adopted values.

Table 5. Nebular temperatures<sup>a</sup>

Diagnostic	(1)	(2)	(3)	(4)	(5)	(6)
$T(\text{Bac})$	8340 ± 500	7100 <sup>+1200</sup> <sub>-900</sub>	6800 ± 400	...	...	6800 ± 400
$T(\text{He II})$	6450 ± 1000	...	...	5730 ± 1000	6674 ± 559	6674 ± 559
$T[\text{O III}]$	7990 ± 50	7950 ± 100	...	...	...	7980 ± 50
$T[\text{O II}]$	9500 ± 500	...	...	...	...	9500 ± 500
$T([\text{O III}], [\text{O II}])$	...	...	...	...	8100 ± 100	8100 ± 100

<sup>a</sup>In K. 1 Wesson & Liu (2004); 2 Kingsburgh et al. (1996); 3 Zhang et al. (2004); 4 Zhang et al. (2005); 5 this paper; 6 adopted values.

Table 6.  $t^2$  values

Method	$t^2$
$T(\text{Bac})$ and $T_e([\text{O II}], [\text{O III}])$	$0.028 \pm 0.009$
$T(\text{He II})$ and $T_e([\text{O II}], [\text{O III}])$	$0.035 \pm 0.014$
$N(\text{C}^{++})_{RL}$ and $N(\text{C}^{+2})_{CEL}$	$0.036 \pm 0.010$
$N(\text{O}^{++})_{RL}$ and $N(\text{O}^{+2})_{CEL}$	$0.024 \pm 0.008$
$N(\text{Ne}^{++})_{RL}$ and $N(\text{Ne}^{+2})_{CEL}$	$0.022 \pm 0.010$
Average	$0.028 \pm 0.005$

Table 7. Stellar and nebular abundances for NGC 6543<sup>a</sup>

Element	Stellar	Nebular (RL)	Nebular (CEL)
He	$11.00 \pm 0.04$	$11.05 \pm 0.01$	...
C	$9.03 \pm 0.10$	$8.90 \pm 0.10$	$8.40 \pm 0.10$
N	$8.36 \pm 0.10$	$8.83 \pm 0.20$	$8.43 \pm 0.20$
O	$9.02 \pm 0.10$	$9.19 \pm 0.12$	$8.79 \pm 0.06$
S	$7.57 \pm 0.10$	...	$7.08 \pm 0.06$
Ne	...	$8.67 \pm 0.10$	$8.25 \pm 0.06$

<sup>a</sup>In units of  $12 + \text{Log } N(\text{X})/N(\text{H})$ .